Manuscript Title

Deep learning and cross-species analysis identify the influences of sex and cannabinoid signaling on cerebellar vermis morphology

Abbreviated Title

Author Names and Affiliations

Kylie Black[2*], Brent McPherson[1*], John Hainline[2], Shawyon Baygani[2], Brynna Webb[2], Tristen Meir[2], Amanda Essex[2], Ken Mackie[2], Franco Pestilli[1], and Anna Kalinovsky[2]

[1] Program in Neuroscience, Cognitive Science Program, Program in Neuroscience, Department of Psychological and Brain Sciences, Indiana University, Bloomington, IN, USA

[2] The Gill Center for Biomolecular Science, Program in Neuroscience, Department of Psychological and Brain Sciences, Indiana University, Bloomington, IN, USA

*Equally contributing first authors

Author Contributions

Kylie Black – ORCID: 0000-0001-6144-6864 – performed research: mouse anatomy and behavior – designed experimental protocols, performed experiments, processed and analyzed data

Brent McPherson – ORCID: 0000-0001-8378-8136 – performed research: human anatomy, machine learning – designed experimental protocols, performed experiments, processed and analyzed data

John Hainline – performed research: mouse behavior, mouse anatomy, HCP data mining, data analysis

Shawyon Baygani – ORCID 0000-0003-4007-2714: – performed research: developmental mouse anatomy, analyzed data

Brynna Webb – ORCID: 0000-0002-9207-2196 – performed research: adult mouse anatomy and behavior

Tristen Mier – ORCID: 0000-0002-9251-4599 – performed research: developmental mouse anatomy, analyzed data

Amanda Essex – ORCID: 0000-0001-5482-9082 – performed research: developmental mouse anatomy

Ken Mackie – ORCID: 0000-0001-8501-6199 – assisted in the design of mouse experiments and interpretation of mouse experimental results.

Franco Pestilli – ORCID:0000-0002-2469-0494 – designed deep learning and human anatomy experiments, directed project.

Anna Kalinovsky – ORCID: 0000-0003-3793-052X – designed experiments, directed project, and wrote manuscript

All authors discussed the results and commented on the manuscript.

Correspondence
Anna Kalinovsky, Psy. & Brain Sciences, IU Bloomington, MSBII Rm. 208, 702 N. Walnut Grove Ave., Bloomington, IN 47405

Acknowledgements
We are grateful to Jim Powers and the IUB Light Microscopy Imaging Facility, and our wonderful undergraduate research assistants Alexandria Bell, Alexander Buchanan, Wesley Cha, Luis Dominguez, Jacob LaMar, Athanasios Liodos, Thomas Metcalf, and Jonah Wirt. Our thanks to all our lab members for discussing this manuscript. This work was supported by NIDA (Grant No. R21DA044000).

Deep learning and cross-species analysis identify the influences of sex and cannabinoid signaling on cerebellar vermis morphology

ABSTRACT

The cerebellum is the only folded cortical structure present in both rodents and humans, potentially allowing mechanistic studies across species. We trained a deep convolutional neural network to predict biological sex from midline cerebellar MRI images, and identified anterior midvermis lobules and white matter as morphological determinants of sex by heatmap backpropagation. Our comparative cross species analysis shows that in mice, like in humans, the extent of anterior vermis folding and the shapes of white matter exhibit sex-dependent differences. In both species, sex and anterior vermis folding patterns influence hand/forelimb dexterity, nevertheless, neither sex nor the extent of folding are good predictors of an individual's behavior, because the variability in performance between individuals is far greater than the differences between conditions. Finally, utilizing mice constitutively lacking CB1 cannabinoid receptors, we identify developmental cannabinoid signaling as a novel molecular mechanism limiting secondary fissure formation.

Anatomical

Vermal Foliation Patterns Distinguish Males and Females

HUMAN

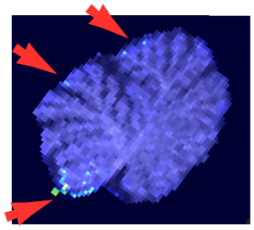

MOUSE

Cross-species analysis showing that patterns of cerebellar vermis foliation are influenced by sex in both mice and humans

Behavioral

Individual Variability in Behaviors is Influenced by Sex and Vermal Foliation Patterns

HUMAN

MOUSE

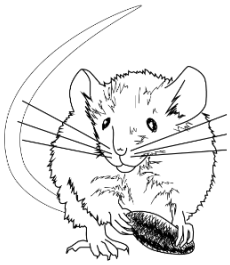

Identifying correlations in anatomical and behavioral variability between individuals

Developmental, Genetic

Knockout of CB1 leads to increased vermal foliation

CB1 +/+

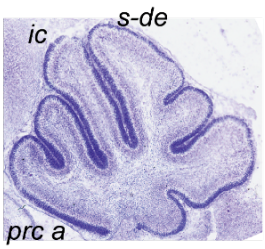

CB1 -/-

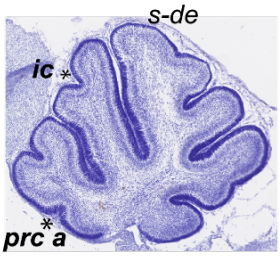

Identifying genetic-developmental mechanisms regulating formation of secondary fissures

INTRODUCTION

From ancient times, humans have been fascinated by the intricate folding of their brain and how it may correlate with differences in individual behaviors: ancient Egyptian papyrus transcribed in the 7th century BC contains description of the folded brain appearance “like ripples that happen in copper through smelting” (Kandel, 2013). In colloquial Russian, “missing a few brain folds” implies that the person is not very smart. In fact, variability in cortical folding accounts to a large extent for the individual variability in brain anatomy (Duan et al., 2020). However, genetic and signaling mechanisms regulating development of folding patterns characteristic of each individual are not well understood. Even though anatomical boundaries of lobules do not always correspond with the boundaries of functional cerebellar subregions (King et al., 2019), they create physical constraints on neuron migration and development of neural microcircuits (Legué et al., 2016). Variability in cerebellar folding has been linked to differences in behavioral outputs in human neurodevelopmental disorders (D’Mello et al., 2015), and in the variability of behavioural complexity between species (Hall et al., 2013).

The cerebellum is a tightly folded cortical structure, its flattened area equalling about 80% of the area of the human cerebral cortex, yet it contains a greater number of neurons (Sereno et al., 2020), and is implicated in a wide range of cognitive, emotional, and motor behaviors (Jacobi et al., 2021). It exhibits intricate anatomical and functional compartmentalization, including rostro-caudal folding of the vermis into ten primary lobules, which are conserved across vertebrates, and secondary lobules, which are more variable between species and across individuals within species (Larsell, 1967).

The cerebellum is not considered sexually dimorphic, albeit alterations in cerebellar structure and function in humans have been associated with neuropsychiatric disorders that exhibit higher prevalence or earlier onset in males, including autism spectrum and schizophrenia (Phillips et al., 2015).

Here we report that males and females exhibit differences in anterior cerebellar vermis folding, identifying it as a brain region exhibiting sex-dependent morphological differences in both mice and humans. Furthermore, we show a correlation between differences in the foliation patterns, shapes of the white matter tracts, and performance of motor tasks. However, the differences in performance of these tasks between individuals are much greater than the mean differences between conditions, underscoring that neither sex nor anatomical differences are enough to predict individual's behavior. Furthermore, expression of secondary fissures correlates with better performance in male mice, but poorer performance in female mice, further underscoring the disociation between anatomical and sex-dependent influences on behavior.

Expression of CB1 cannabinoid receptors in the anterior vermis of mice is high around birth, and decreases during the first postnatal week, at the time when secondary fissures are initiated (Martinez et al., 2020). Here we show that CB1 is required for regulation of the timing of formation and the abundance of secondary fissures in mice, highlighting a previously unrecognized role of cannabinoid signaling as a molecular mechanism regulating cortical folding.

Utilizing a cross-species approach in this work allowed us to bridge multiple levels of analysis: from behavioral, to anatomical, to molecular signaling shaping brain development. The results reported here highlight advantages and limitations of using this approach to the study of the age-old fundamental question of the relationship between shape and function.

RESULTS

Predominant Pattern of Vermis Foliation is Sex-Dependent in CD1 Mice. In his classical work, Olof Larsell analyzed foliation patterns of multiple vertebrate species, identifying ten primary vermal lobules (I-X), conserved in the majority of vertebrates (Larsell, 1967). Using Larsell's classical anatomical criteria, lobules II, III, V, VI, VII, VIII, IX, and X can be consistently recognized in all CD1 mice (Fig. 1 A-A"). Per Larsell's nomenclature, lobe I is a half-lobe nested on the dorsal surface of the anterior medullary velum and is characterized by its white matter resting directly on the velum. Guided by this definition, lobe I (fig. 1A" – a fissure separating lobe I from lobe II is marked by green arrowhead) is extremely rare in CD1 mice (1/100 in our colony – that is in contrast to the C57B6 inbred strain that was not used in our study). In CD1 mice, a high individual variability in foliation patterns is prominent in three midvermal regions: (1) fissure *precentral-a* (*prc-a*) separates lobe II into lobules IIa and IIb in some animals, but others exhibit an undivided lobe II; (2) *intra-culminate* (*ic*) fissure, separating lobules IV and V, is present in some and absent in other animals; (3) in some animals a *superior-declive* (*s-de*) fissure is present dividing lobe VI into VIa and VIb. Sites of these secondary fissures are marked by green-lettered abbreviations, and when the fissure is

present it is indicated by an asterisk (Fig. 1 A-A”). Anatomical nomenclature was adopted from (Larsell, 1967), (Inouye & Oda, 1980).

Since secondary fissures are variable between individuals, we asked what factors governing cerebellar development may increase the probability of secondary fissure formation. A ubiquitous genetic mechanism contributing to variability between individuals within vertebrate species is biological sex. Thus, we examined the relationship between sex and the prevalence of secondary fissures in CD1 mice. Our results show that more males than females exhibit any of the three most common secondary fissures: *prc-a*$^+$ – 53% of males vs. 43% of females, *ic*$^+$ – 50% of males vs. 40% of females, *s-de*$^+$ – 66% of males vs. 49% of females (Fig. 1 B). Males are more likely to express multiple secondary fissures (males are 3 times more likely than females to express all three secondary fissures, while females are twice more likely than males to express no secondary fissures at all, Fig. 1 C). Thus, the cerebellar vermis exhibits sex-dependent foliation differences in CD1 mice – males are characterized by a higher probability to express any of the secondary fissures, and a higher total number of secondary fissures as compared to females.

Increased Foliation is Independent from Differences in Vermal Size. Increased foliation and larger cortical size have been positively correlated in prior studies (Corrales et al., 2006)(Kim & Scott, 2014; Whittaker et al., 2017). In order to elucidate whether increased foliation in males may be linked to increased cerebellar vermis size, we measured the size of the midvermal area, and found it to be slightly larger in males (Fig.

1 D – 12 mm^2 mean in males and 11 mm^2 mean in females, P=0.02). This difference of means between sexes is many folds smaller than the distribution of values within each sex (from less than 8 to about 16 mm^2), and is erased when midvermal area is normalized to animal weight (Fig. 1 E). Most importantly, in both males or females, the presence of the secondary fissure *prc-a* does not correlate with differences in midvermal area (Fig. 1 D).

Since the majority of differences in foliation localize to the anterior zone (AZ, rostral from the primary (*prm*) fissure, purple dotted outline in Fig. 1 A-A”), we assessed the differences in the anterior zone area and the ratio of anterior zone to total midvermis between animal with or without *prc-a*, and found none (Fig. 1 F, G). In conclusion, CD1 male mice exhibit increases in the prevalence of secondary fissures *prc-a*, *ic*, and *s-de*, but the prevalence of secondary fissures does not correlate with increases in total, or anterior, vermal area, suggesting that increased foliation depends on a mechanism independent from the increase in cortical size.

Differences in the Foliation Pattern Affect the Shape of Interlobular White Matter Tracts. Cerebellar cortex is composed of morphologically, cellularly and functionally distinct layers: the outermost molecular layer (ML), underlied by the Purkinje cell layer (PCL), with the inner granule cell layer (IGL) located in the innermost portion of the cerebellar gray matter, resting on top of the white matter (WM). Animals expressing secondary fissure *prc-a* (prc-a^+) have distinctly different overall shape of lobules II-III as compared to animals who do not (prc-a^-): the former resembling a trefoil leaf versus a

two-prong fork (Fig. 2 A). However, it is not clear whether these differences in the general shape reflect local differences in the size and composition of the gray and the white matter. To evaluate what structural elements of cerebellar cortex are affected by expression of secondary fissures, we quantified areas of the layers in lobules II-III from midsagittal sections (Fig. 2 A). In both females (Fig. 2 B-G) and males (Fig. 2 H-M), we found no significant differences between prc-a$^-$ and prc-a$^+$ in the mean ML area (Fig. 2 B, H), the mean IGL area (Fig. 2 C, I), PCL length (Fig. 2 0), or spacing of Purkinje cells (Fig. 2 P). Thus, the differences in the overall shapes of lobules II-III do not correspond to differences in the size of the layers composing cerebellar gray matter.

On the other hand, the WM area of lobules II-III is significantly smaller in prc-a$^+$ as compared to f prc-a$^-$ females (Fig. 2 D, p=0.0007). Smaller WM area in prc-a$^+$ females could be a consequence of either reduced length, or reduced width of WM fascicles. We measured the length of WM fascicles projecting into individual folia (IIa in prc-a$^+$ or the apex of the corresponding WM bulge in prc-a$^-$; IIb; and III – punctate lines in Fig. 2 A). There is a trend for slightly shorter II/IIb and III WM tracts in females, but it is not statistically significant (Fig. 2 F and G). Conversely, IIa WM tracts exhibit a trend to be longer in prc-a$^+$ females (Fig. 2 E). Thus, the most likely reason for smaller WM area in prc-a$^+$ females is reduction in the width, but not the overall length, of WM tracts.

In males, no differences in WM area are observed between prc-a$^-$ and prc-a$^+$ (Fig. 2 J). However, the increased length of IIa WM in prc-a$^+$ males is statistically significant (Fig. 2 K, p=0.0007). Thus, increased vermal folding is associated with structural changes in

cerebellar white, rather than gray, matter: with overall “slimmer” (thinner in females, and longer in males) WM tracts.

Correlation between Vermis Foliation and Cerebellar-Influenced Sensorimotor Behaviors Shows Opposing Trends in Females and Males. Anterior cerebellar vermis receives projections from motor, somatosensory and vestibular afferents, and is activated during tasks that involve forelimb and hindlimb dexterity and balance (Jacobi et al., 2021), (Coffman et al., 2011), (Chambers & Sprague, 1955). We wondered whether behaviours associated with anterior cerebellar vermis may exhibit sexual dimorphism in humans. Analysis of behavioral data from the human connectome project (HCP, https://www.humanconnectome.org) shows that in a forelimb dexterity task (peg sorting) males are slightly faster than females (Fig. 3 A). Importantly, this analysis also highlights a wide variability in performance between individuals, that is many folds greater than the differences in mean performance between sexes, Humans do not exhibit detectable sex differences in the gait test (Fig. 3 B).

Since the anterior cerebellar vermis is characterized by sex-dependent differences in foliation, we asked if CD1 mice exhibit sex-dependent differences in performance of cerebellar-influenced behaviors. We assessed forelimb dexterity in CD1 mice in the sunflower seed opening task. As in humans, male mice also show a trend to complete the task faster, and large variability is evident between individuals (Fig. 3 C). Since presence of secondary fissures is more common in males, could seed opening performance correlate with their presence? Looking at the correlation between seed

opening times and the presence of *prc-a* (Fig. 3 C), *ic*, and *s-de* (Fig. S-1 A), we found opposing trends between sexes but no statistically significant differences. We assessed whether the length of IIa WM correlates with performance in seed opening task, and found a positive correlation in males, and a negative correlation in females, as shown by linear regression analysis (Fig. 3 D; males: $y = -48 X + 70.46$, R^2 males = 0.221; females: $y = 83 X + 7.86$, R^2 females = 0.313; p=0.0011).

Rotarod (balancing on a rotating accelerating beam) is a standard behavioral test in mice used to assess sensorimotor coordination and learning. We found no overall differences in rotarod performance regardless of sex or variation in lobe 2 foliation (Fig. 3 E). The rate of learning, improvement from the first to the last trial, or latency to fall relative to IIa WM length do not differ between conditions (Fig. S-1 B-E). We defined "top performers" in rotarod as being able to stay on the rotating rod >80% of maximum time (240-300s). During later trials (after trial 5) a relatively stable proportion of animals are "top performers" in each group. Intriguingly, there are about two-fold more top performers on trials 5-12 among prc-a^- males vs. prc-a^+ males (Fig. 3 H, ~40% vs. ~20%). The trend is inverted in females, with fewer top performers in prc-a^- females compared to prc-a^+ (Fig. 3 H, ~40% vs. ~60%). Thus, high-level performance in rotarod does correlate with foliation, with opposite trends between sexes: top performing males exhibit less foliation, while top performing females exhibit more.

In conclusion, mice exhibit a correlation between the mesoscale anatomical characteristics of anterior cerebellar vermis – the extent of foliation and the shapes of

IIa WM tracts – and two sensorimotor tasks that are under the influence of anterior cerebellar vermis: seed opening and proficiency in rotarod – and the effects are notably inverted between sexes. While prc$^+$ males perform better than prc$^-$ males, the opposite trend is seen in females.

Cannabinoid Signaling Regulates Development of Secondary Fissures. Primary fissures, which are conserved between individuals and in the majority of vertebrate species, are initiated early in development, elongating while cerebellar cortex undergoes a several-fold expansion, becoming deeper and more pronounced compared to the secondary fissures which are initiated later (Sudarov & Joyner, 2007), (Legué et al., 2015), (Ma et al., 2012). We have characterized the developmental time course of secondary fissure formation in CD1 mice. In wildtypes (WTs) secondary fissures *prc-a*, *ic*, and *s-de* are initiated after postnatal day 3 (P3) (Fig. 4 A, B, C, D, E). A higher percentage of males consistently exhibit secondary fissures at earlier time points:

prc-a – at P5 10% of males and none of females exhibit *prc-a*; at P10 ~21% of males but only ~18% of females are prc-a$^+$, and the proportion of prc-a$^+$ animals increases with age in both sexes, at two-month-old (2mo) reaching ~53% in males and ~43% in females (Fig. 4 C).

ic – at P5 ~30% of males and ~20% of females express *ic*, reaching ~50% in males and ~40% in females by P10-2mo (Fig. 4 D).

s-de – at P5 ~40% of males and ~25% of females express *ic*, and by P10 the maximum proportion of s-de$^+$ (~75%) is reached for both sexes (Fig. 4 E).

Thus, the higher prevalence of secondary fissures in males may be a consequence of an earlier and longer developmental window for secondary fissure initiation.

Strikingly, in constitutive CB1 cannabinoid receptor knockouts (KOs) , majority of animals of both sexes exhibit anterior zone secondary fissures *prc-a* and *ic* (Fig. 4 A', B', C, D). Conversely, there is no difference between WTs and CB1 KOs in the prevalence of *s-de*, located in the central zone (Fig. 4 E). Furthermore, *prc-a* and *ic* are initiated prematurely in CB1 KOs: by P3 ~100% in males and ~73% of females are prc-a^+, and ~75% of males and ~27% of females are ic^+ (Fig. 4 C, D). Thus, cannabinoid signaling through CB1 limits the formation of secondary fissures by delaying the developmental window during which secondary fissures can be initiated. Consequently, increased foliation due to the common occurrence of secondary fissures in the anterior zone is a distinguishing morphological feature of CB1 knockouts.

Human sex is well predicted using cerebellar anatomical images.

Based on postmortem examination of human brain tissue, Olof Larsell has established 50 years ago the nomenclature for human vermal lobules in relation to other species (Fig. 5 A, from "Human Cerebellum" figure 55 B, p.45;(Larsell, 1967)). The high degree of variability in midvermal foliation in humans, and in particular the variability in appearance of lobules I-II was emphasized in that study (Fig. 5 B, from "Human Cerebellum" figure 54, p.41; (Larsell, 1967)). This high degree of variability is also evident in MRI scans from HCP (Fig. 5 C). We asked whether in humans the foliation pattern of cerebellar vermis is influenced by sex, similarly to the mouse.

Since human cerebellar vermis exhibits much higher degree of foliation variability compared to mice, and because the imaging resolution of MRI scanning is lower compared to classical histological staining and microscopy, it is impractical to conduct the same type of morphometric analysis as we conducted for the mouse cerebella from human scans. Thus, we chose to use an unbiased approach to probe for anatomical differences.

Midline sagittal images were cropped and masked in order to limit analysis to midvermal cerebellum (Fig. 5 C). Labels from the SUIT atlas were moved to the subject's native space after alignment to identify the midline sagittal plane (J. Diedrichsen et al., 2009), (Jörn Diedrichsen, 2006), (J. Diedrichsen et al., 2011). All pixels outside the label set were zeroed so no confounding information from surrounding tissue would contribute to the prediction. Images were passed through multiple layers of convolutional filters. The filters initially describe the local patterns found in the image, but as the layers later in the model become smaller they represent more global properties of the image. The decision layer used the combined weights from all the previous layers to make the desired category assignment (Fig. 5 D). The network was trained for 500 epochs on samples from the training set of the data. The accuracy for the training data never consistently surpassed the validation data, indicating the data is not over-fit and should generalize well to new samples (Fig. 5 E). The best accuracy achieved was 93% (Fig. 5 E).

Specifically, a deep convolutional neural network (CNN) was trained using Keras and validated on a 66% / 34% split of the HCP data. Images were taken of a midline slice of the cerebellum after registering labels from the SUIT atlas to the subjects space and passed through an intensity normalization process that scaled the images for training (J. Diedrichsen et al., 2009), (Jörn Diedrichsen, 2006), (J. Diedrichsen et al., 2011). The images acquired were 850 pixels square and masked all but the voxels appearing in the cerebellum to zero. Images were passed through a series of 6 2D convolutional filters and combined with pooling layers (filter sizes = 8, 16, 32, 64, 128, 256; kernel size = (3, 3); RELU activation). A dense connection layer with a RELU activation function (250 nodes) using a 50% dropout preceded a sigmoid activation function to make the final classification of gender. The model was built using the root-mean-square propagation (RMSprop) optimization with a binary cross-entropy loss function (learning rate = 0.0001). The model was run for 500 epochs with 32 training and test steps per epoch. Prediction accuracy was used as a metric to evaluate model performance.

What regions of cerebellar vermis contribute to sex-dependent anatomical differences? we assessed saliency of each voxel of the MRI in predicting sex (backpropagated heatmap) marking anatomical locations contributing the most to the sex-dependent differences, which highlighted the same anterior vermis variable lobules that the morphological analysis in mice identified as contributing to sex-dependent differences in folding (Fig. 5 F).

Thus, in humans, as well as in mice, cerebellar vermis exhibits sexual dimorphism in the extent of foliation.

DISCUSSION

Advancements in the development of non-invasive brain imaging methodology and the computational tools for anatomical shapes analysis has renewed interest in the age-old fundamental neuroscience question of shape-function relationship; and thus renewed the hope to find non-invasive imaging biomarkers that can be utilized in the diagnosis and prognosis of neurological and psychiatric conditions.

Sex is an important biological variable affecting multiple aspects of nervous system development: from regulation of programmed cell death and gene expression to differences in basal levels of neuronal and neuroendocrine activity, to different sizes of brain regions regulating dimorphic reproductive behaviors (reviewed in (McCarthy, 2016)). Yet, these effects have been documented only in a few select brain regions. Beyond general scaling of cerebellar size with the body size, leading to slightly larger cerebella in males (Raz et al., 2001), and difference in expression levels of calcium binding protein (Calb) in cerebellar Purkinje cells (Abel et al., 2011), sex has not been considered to influence cerebellar development, function or morphology.

Therefore, we were surprised by our initial observation that in mice the prevalence of secondary fissures, and thus the predominant folding pattern in the anterior cerebellar vermis, differ between sexes. We used large open-access MRI database containing

brain images from 1200 healthy subjects (HCP), with analysis limited to the cerebellum, trained 2D convolutional neural network on midsagittal slices, and achieved >93% accuracy in prediction of sex, highlighting that human midvermis is a sexually dimorphic brain region. Heatmap backpropagation identified secondary fissure sites in the anterior vermis as the morphological features primarily determing differences between men and women. Our results demonstrate that in both mice and humans, biological sex influences the folding pattern of anterior cerebellar vermis, expanding the cohort of brain regions known to harbor sex-dependent morphological differences.

What are the functional consequences of individual variability in folding patterns? Neurosurgeons and radiologists use the pattern of cortical folding as anatomical landmarks, so assessment of variability between individuals in prevalence of specific fissures, and general understanding of the differences in that prevalence between sexes, are beneficial for clinical applications. Nevertheless, a large extent of individual variability is apparent in the boundaries of functional regions relative to fissure locations. Is there any correlation between individual variability in gross anatomical parameters, such as the folding pattern, and individual variability in behavioral outputs?

We hypothesized that the continuum in the extent of anterior vermis folding may correlate with the continuum of variability in forelimb dexterity, and that this shape-function relationship may be a good predictor of behavior (rather than the split into female versus male). We assumed that biological sex may influence anterior vermis foliation through its effect on developmental mechanisms, and sex-dependent

differences in behavior may be secondary to the morphological differences. Importantly, our results do not support this hypothesis: the correlation between the extent of anterior vermis folding and the proficiency in forelimb dexterity tasks is flipped in females versus males. Interestingly, the predominant folding pattern in females (fewer fissures) correlates with better performance in the forelimb dexterity task for females, while the opposite – more secondary fissures – correlates with better performance in males, suggesting that in the combinatorial and multifactorial processes that regulate brain development and function, similar functional outcomes could be achieved even when some of the starting parameters are very different. This highlights the dissociation between the influence of biological sex on the development of cerebellar morphological features, and the influence of morphological features on behavior. In addition, it highlights the naïveté of the expectation that morphological differences alone could provide predictive behavioral markers – however, the prediction improves when additional biological determinants, such as sex, are considered. In sum, our results show that both sex and foliation patterns influence specific parameters of well defined, cerebellar-influenced behaviors. However, for all behaviors assessed, far greater variability is observed between individuals within each sex and foliation category, than the mean differences between categories, underscoring the complexity of the relationship between sex, extent of foliation, IIa WM length, and cerebellar-influenced behaviors.

The size, shape, and extent of connectivity between brain regions create anatomical constraints to the numbers of cells and the patterns of neuronal connectivity. To bridge

the gap in understanding how the differences in the extent of anterior cerebellar vermis folding may influence behaviors, we performed morphological analysis of the different, cytologically distinct, cerebellar layers. Surprisingly, the differences in the extent of folding do not cause detectable differences in the areas of any of the cerebellar cortical layers, but do affect the shape of white matter tracts, promoting “slimmer” white matter bundles. Multiple factors can lead to a decrease in WM shape, including changes in the packing of long-range axons within the WM fascicles, changes in the number of oligodendrocytes or the extent of myelination. Cellular mechanisms associated with the sex-dependent differences in overal WM shape would be interesting to explore in the future. Another question suggested by our results is whether variability in WM tracts’ shape may be associated with variability in accuracy of timing in cerebellar-controlled behaviors?

What are the biological mechanisms regulating folding?

Biological sex is just one of the factors to influences development of anterior cerebellar vermis folding. In this work we identify developmental cannabinoid signaling as a key mechanism limiting formation of secondary fissures in the anterior cerebellar vermis. In CB1 KO mice, both males and females express super-numerous secondary fissures. Endocannabinoid signaling plays important roles in brain development and early life exposure to phytocannabinoids is considered a risk factor for the development of schizophrenia, emotional and attentional deregulation, and substance use disorder (Bara et al., 2021). The most abundant neuronal cannabinoid receptor, CB1, is expressed during cerebellar development; CB1 expression in WM in mouse anterior

cerebellar vermis rapidly decreases in the first few days after birth (Martinez et al., 2020) – just before the developmental window of *prc-a* and *ic* initiation. This raises several important questions: Is downregulation of CB1 or of cannabinoid signaling through CB1 required for the initiation of secondary fissure formation? Does the timing of this downregulation control the prevalence of secondary fissures? Can prenatal exposure to cannabis influence cerebellar folding? Cerebellar function and cerebellar-influenced behaviors later in life?

Initiation of fissure development has been proposed to depend on the formation of developmentally transient structures: fissure anchoring points, generating physical constraints of cortical expansion by constraining neuronal migration through tight junctions between the endfeet of Bergman glia and the invaginated basilar membrane (Sudarov & Joyner, 2007), (Legué et al., 2015), (Ma et al., 2012). In the future it would be interesting to explore whether cannabinoid signaling is potentially involved in regulation of these cellular behaviors during development.

MATERIALS AND METHODS

Mouse Colony: All mice used in this study were maintained on an outbred CD1 genetic background. The CD1 IGS stock was acquired from Charles River, USA (https://www.criver.com/products-services/find-model/cd-1r-igs-mouse?region=3611), and replenished by purchasing additional CD1 breeders from Charles River once a year. Breeding colony was maintained in the vivarium at Indiana University, Bloomington with 12-hour light/dark cycle under conditions stipulated by the Institutional

Animal Care and Use Committee. *cb1* -/- mice (CB1 KO) used in this study were generated by (Ledent, Valverde et al. 1999), acquired from Charles River France. CB1-KOs were kept as outbreed colony on CD1 background by breeding heterozygous CB1+/- with CD-1 WTs. First degree crosses (siblings, parents, etc.) were always avoided.

Tissue Sectioning and Nissl Staining: Mouse brain tissue was fixed by perfusion followed by post-fixation in 4% paraformaldehyde (PFA). 20 μm sagittal sections were serially collected using a cryostat (Leica). Nissl staining was performed following a standard protocol. In short, following PBS and dH2O washes, sections were incubated in 0.1% Cresyl Violet solution, followed by dehydration, clearing in xylene, and mounting in Permount. Images of whole cerebellar sections were obtained using 4x objective and mosaics with an Applied Precision DeltaVision Nikon microscope and Motic EasyScan at IUB Imaging Facility. Figures were prepared in Adobe Photoshop and Adobe Illustrator.

Immunohistochemistry: For immunohistochemistry brain sections were washed 3 times in 1X PBS and incubated in BSA blocking buffer (5% BSA; 0.5% Triton x100; 1X PBS). Anti-calbindin (Rabbit anti Calb, Swant, #CB38, RRID: AB_2721225) primary antibody was applied overnight at 4˚C in BSA blocking buffer at 1:3000 dilution. Subsequently, slides were washed 3 times in 1X PBS and secondary antibodies (Alexa Flour 488 from Jackson ImmunoResearch) were applied at 4˚C overnight (1:600 in BSA blocking buffer). DraQ5 (Cell Signaling) was used (at 1:5000 in PBS) to visualize cell nuclei. Slides were coverslipped using Fluoromount G (SouthernBiotech).

Morphological Analysis: Areas of interest were traced from midsagittal sections using free-hand tool in FiJi (https://imagej.nih.gov/nih-image/manual/tools.html). Statistical Statistical Analysis: (Figures 1 and 2). Statistical analysis was performed in GraphPad Prism 9 (www.graphpad.com). Data was collected from 111 two-month-old mice of both sexes, from 28 distinct liters. Statistical hypothesis tested magnitude of differences in area means between males and females with and without *prc-a*. P-values and 95% confidence intervals of difference were evaluated by 2way AVOVA, or multiple T tests when appropriate.

Mouse Behavior: Rotarod: Two-month-old mice were placed on an accelerating rotarod (UGO Basile) which accelerated from 4 to 40 rpm over a 5 minutes period. The latency until the mouse fell off was recorded. Mice were given three trials over four consecutive days with a maximum time of 300 seconds (5 minutes) per trial and given 15 minutes to recover between trials. Statistical Analysis: (Figures 3 and S-1). Statistical analysis was performed in GraphPad Prism 9 (www.graphpad.com). Data was collected from 27 females and 28 males (7 liters) over a time course of 12 trials (3 per day). Statistical hypothesis tested magnitude of differences in latency to fall between sexes with and without secondary fissures. P-values and 95% confidence intervals of difference were evaluated by 2way AVOVA, or multiple T tests when appropriate. Improvement in rotarod performance was evaluated by fitting linear regression curves over the first six trials, and differences in slopes between groups were compared. In addition, for each animal, performance in trial 1 was compared with performance in trial 12. Correlation between IIa length and performance in the last rotarod trial was

evaluated by linear regression analysis. Ratio of top performers (staying on the rod >80% of total time, i.e. 270-300 seconds) was calculated for trials 5-12.

Seed Opening: Two-month-old mice were food deprived overnight (12 hours), and then placed in the testing cage with 4 seeds. For each seed, time was recorded from first contact with the seed and until the mouse stopped interacting with the seed. Only trials in which the seed was opened and at least 75% consumed were included in the analysis. Data for each mouse is the average time to open 2-5 seeds. Statistical Analysis: (Figures 3 and S-1). Statistical analysis was performed in GraphPad Prism 9 (www.graphpad.com). Data was collected from 25 female and 27 male animals (7 liters). Statistical hypothesis tested magnitude of differences in seed opening latencies between sexes and depending on the expression of secondary fissures. P-values and 95% confidence intervals of difference were evaluated by 2way AVOVA, or multiple T tests when appropriate. Correlation between IIa length and latency to open seeds was evaluated by linear regression analysis.

Human Behavior: Data was taken from the Human Connectome Project (HCP) database (https://www.humanconnectome.org). Peg sorting: time required to accurately place and remove 9 plastic pegs into a plastic pegboard, including 1 practice and 1 timed trial with each hand. Raw scores are recorded as time in seconds that it takes the participant to complete the task with the dominant hand. Gait: This test is adapted from the American Thoracic Society's 6-Minute Walk Test Protocol. This test measures the distance that the participant is able to walk on a 50-foot (out and back) course in 2 minutes. The participant's raw score was recorded as the distance in feet and inches walked in 2 minutes, shown as an average speed of walking expressed in meters per

second. (Figure 3). Statistical Analysis: Statistical analysis was performed in GraphPad Prism 9 (www.graphpad.com). Statistical hypothesis tested magnitude of mean differences in performance between sexes, T-test analysis was used to compare the two groups.

Deep learning: Midline sagittal images were cropped and masked in order to limit analysis to midvermal cerebellum (Fig. 4 C). Labels from the SUIT atlas were moved to the subject's native space after alignment to identify the midline sagittal plane (J. Diedrichsen et al. 2009; Jörn Diedrichsen 2006; J. Diedrichsen et al. 2011). All pixels outside the label set were zeroed so no confounding information from surrounding tissue would contribute to the prediction. Images were passed through multiple layers of convolutional filters. The filters initially describe the local patterns found in the image, but as the layers later in the model become smaller they represent more global properties of the image. The decision layer used the combined weights from all the previous layers to make the desired category assignment (Fig. 4 D). The network was trained for 500 epochs on samples from the training set of the data. The accuracy for the training data never consistently surpassed the validation data, indicating the data is not over-fit and should generalize well to new samples (Fig. 4 E). The best accuracy achieved was 93% (Fig. 4 E).

Specifically, a deep convolutional neural network (CNN) was trained using Keras and validated on a 66% / 34% split of the HCP data. Images were taken of a midline slice of the cerebellum after registering labels from the SUIT atlas to the subjects space and passed through an intensity normalization process that scaled the images for training (J.

Diedrichsen et al. 2011, 2009; Jörn Diedrichsen 2006). The images acquired were 850 pixels square and masked all but the voxels appearing in the cerebellum to zero. Images were passed through a series of 6 2D convolutional filters and combined with pooling layers (filter sizes = 8, 16, 32, 64, 128, 256; kernel size = (3, 3); RELU activation). A dense connection layer with a RELU activation function (250 nodes) using a 50% dropout preceded a sigmoid activation function to make the final classification of gender. The model was built using the root-mean-square propagation (RMSprop) optimization with a binary cross-entropy loss function (learning rate = 0.0001). The model was run for 500 epochs with 32 training and test steps per epoch. Prediction accuracy was used as a metric to evaluate model performance.

FIGURES

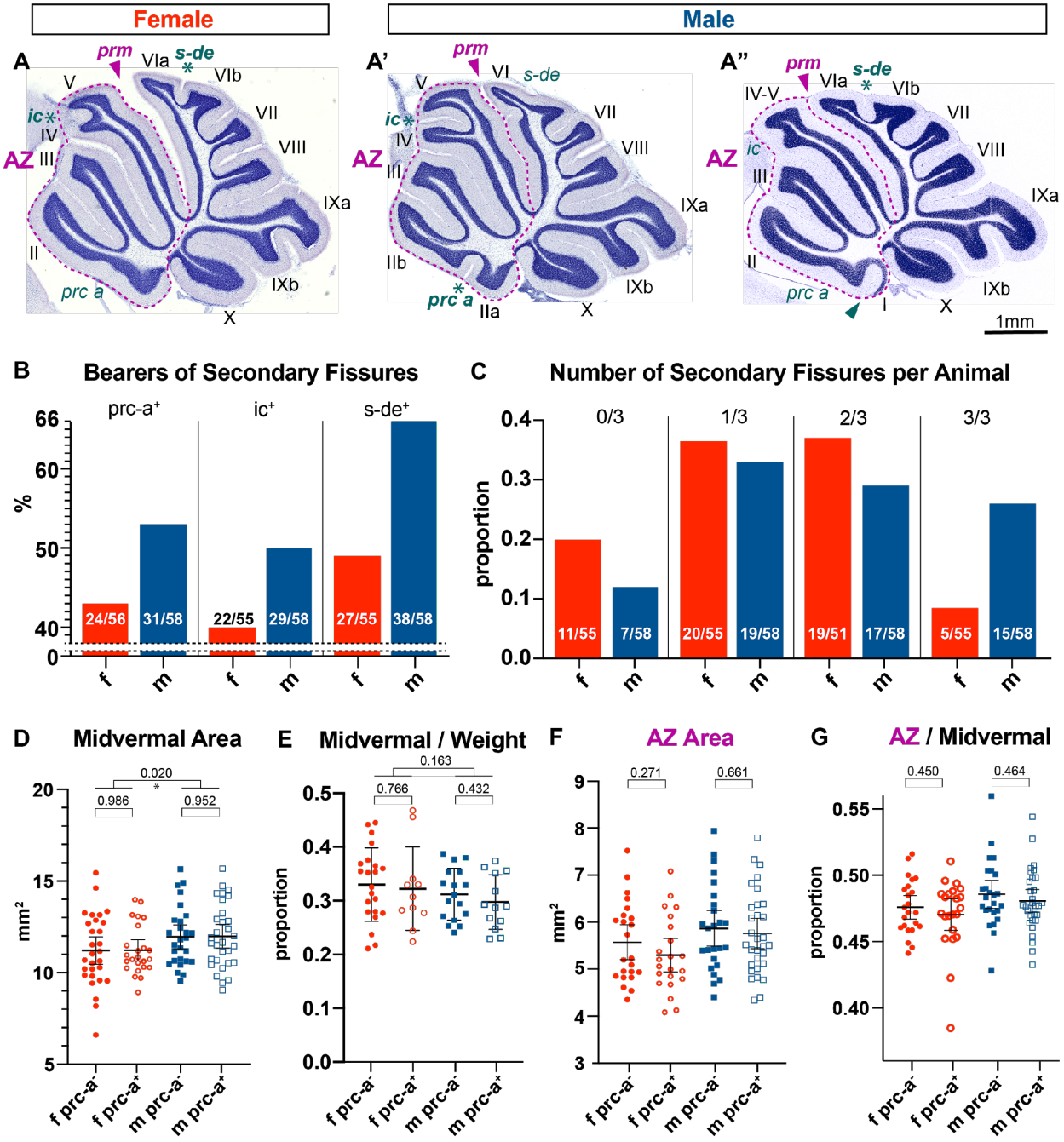
Female
Male
A
A'
A"
prm
s-de
ic
AZ
prc a
1mm
B
Bearers of Secondary Fissures
prc-a+
ic+
s-de+
%
24/56
31/58
22/55
29/58
27/55
38/58
C
Number of Secondary Fissures per Animal
0/3
1/3
2/3
3/3
proportion
11/55
7/58
20/55
19/58
19/51
17/58
5/55
15/58
D
Midvermal Area
mm²
0.020
0.986
0.952
E
Midvermal / Weight
proportion
0.163
0.766
0.432
F
AZ Area
mm²
0.271
0.661
G
AZ / Midvermal
proportion
0.450
0.464
f prc-a-
f prc-a+
m prc-a-
m prc-a+

Figure 1. Secondary fissures in the cerebellar vermis are more prevalent in the male CD1 mice. Representative female **(A)** and male **(A')** midsagittal cerebellar sections. Fissures separate the vermis into lobes (designated by roman numerals). Locations of secondary fissures are shown by green-lettered abbreviations, and by an asterisk when the fissure is present. Purple arrowheads mark the primary fissure (*prm*), a landmark designating the boundary of the anterior zone (AZ) – outlined in purple. **(A")** Shows a rare case where lobe I, a half-lobe nested on the dorsal surface of the anterior medullary velum, can be seen. A fissure separating lobe I from lobe II is marked by a green arrowhead. **(B)** Proportion of animals expressing each one of the secondary fissures (*prc-a*, *ic*, and *s-de*) is higher in males, as well as **(C)** the proportion of animals expressing all three secondary fissures. **(D)** The sizes of total midvermal area exhibit a distribution from less than 5 mm^2 to over 15 mm^2 in two-month-old CD1 mice of both sexes. The average size of midvermal area is about 1 mm^2 larger in males (P=0.02), but the difference between sexes in total midvermal area sizes is no longer apparent when **(E)** midvermal area is normalized to animal weight. Furthermore, for either sex, there are no differences in total midvermal size between animals expressing the secondary fissure *prc-a* (prc-a^+) and those that do not express *prc-a* (prc-a^-). **(F)** Anterior zone area and **(G)** ratio of anterior zone out of total midvermal area do not differ between prc-a^+ and prc-a^- animals. Abbreviations are: AZ – anterior zone of cerebellar vermis, *ic* – intraculminate fissure, *pcen* – precentral, *prc-a* – anterior precentral fissure, *prm* – primary fissure, *s-de* – superior declive fissure. Anatomical nomenclature was adopted from (Larsell, 1967, Inouye & Oda, 1980)

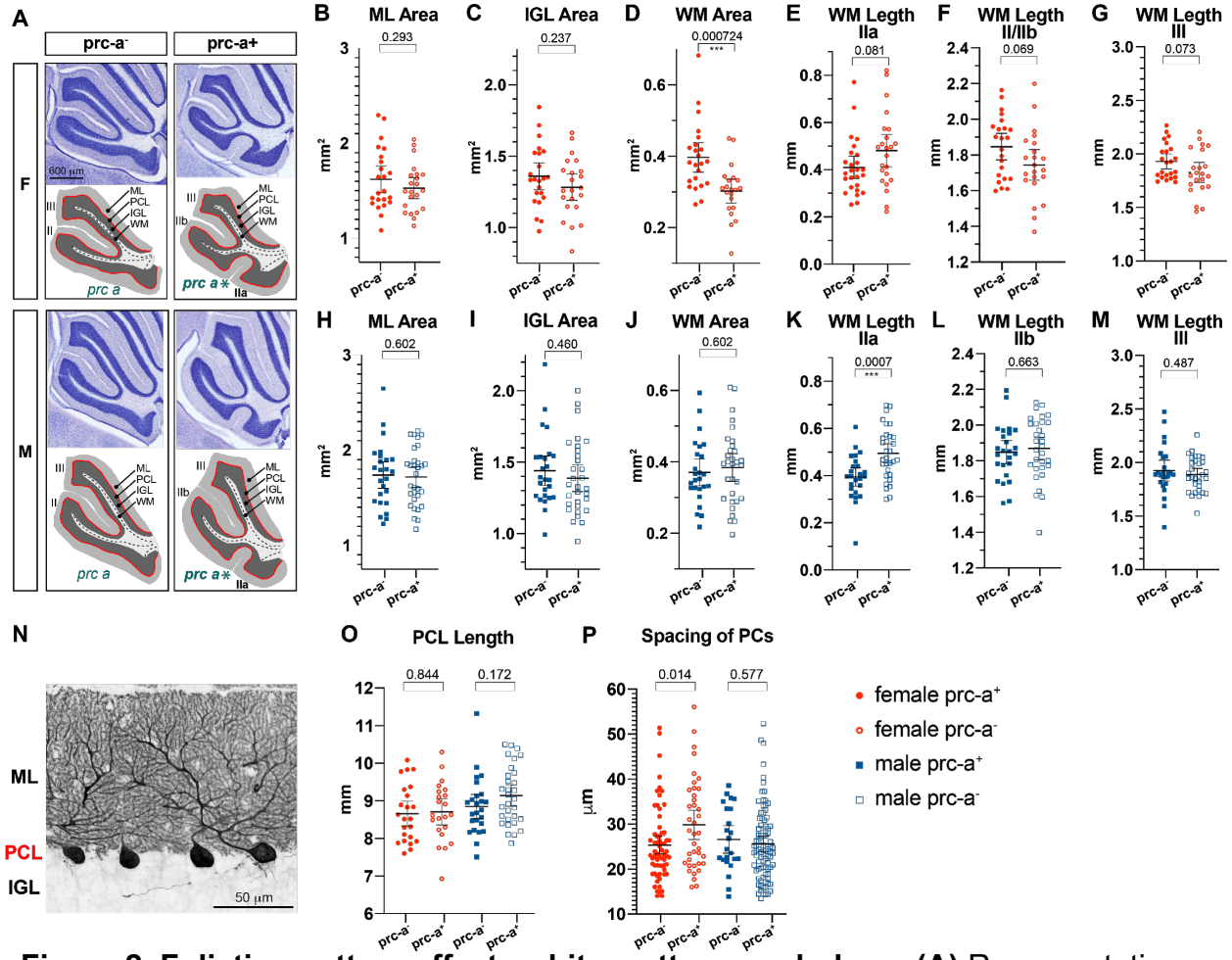

Figure 2. Foliation pattern affects white matter morphology. (A) Representative midsagittal sections showing lobes II-III in anterior zone of cerebellar vermis. Diagrams highlight cerebellar layers: molecular layer (ML), Purkinje cell layer (PCL), inner granule cell layer (IGL), and white matter (WM). Punctate lines trace the course through the middle of WM tracts to the folia apexes that was used to measure lengths of WM tracts. In prc-a$^-$ animals where no distinct lobe IIa is present, the length of IIa WM tracts was estimated by tracing to the apex of the WM that bulges out in the corresponding place. Folia are designated by roman numerals, sites of the secondary fissure *prc-a* by green-lettered abbreviations, and asterisks indicate when the fissure is present. **(B-G)** Quantification of areas of cerebellar layers and lengths of WM tracts in lobes II-III in females, and **(H-M)** in males. **(N)** Calb immunolabeling was used to quantify spacing between adjacent Purkinje cells. **(O)** Quantification of total PCL length in midsagittal sections lobes II-III. **(P)** Quantification of spacing between adjacent Purkinje cells on the ventral side of lobe II. Abbreviations: IGL = inner granule cell layer, ML = molecular layer, PCL = Purkinje cell layer, WM = white matter, *ic* = intraculminate fissure, *pcen* = precentral, *prc-a* = anterior precentral fissure, *prm* = primary fissure, *s-de* = superior declive fissure, F = female, M = male.

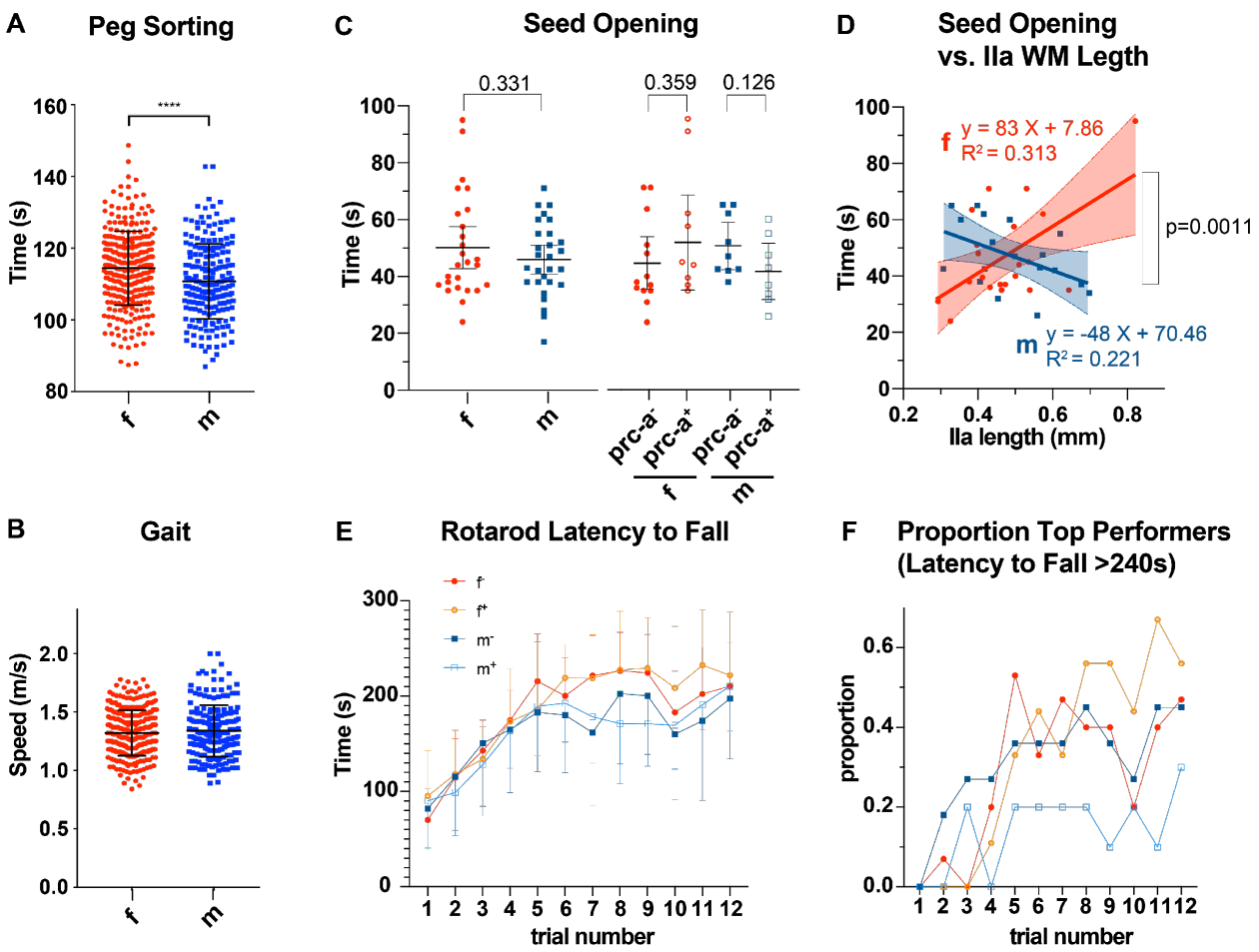

Figure 3. The Extent of Folding in the Anterior Vermis Affects Behavioral Performance, Showing Opposing Trends in Females and Males (A) Human subjects performing peg sorting task (data from HCP). Y-axis shows time (in seconds) required to accurately place and remove 9 plastic pegs into a plastic pegboard with a dominant hand. **(B)** Human subjects performing gait test (data from HCP).The Y-axis shows the participant's average walking speed (recorded for 2 minus while walking comfortably on a walkway) in meters per second. **(C)** Mouse sunflower seed opening task. Average time (in seconds) it takes a mouse to open a sunflower seed. Male mice, like human males, finish the forelimb dexterity task on average slightly faster. Parsing out the mouse seed opening data by the presence of *prc-a*, shows opposing trends between sexes: prc+ females trend to take longer, while prc+ males trend to take shorter time to open seeds, as compared to their prc- counterparts. **(D)** Correlation between performance and length of IIa WM between males and females. **(E)** Rotarod latency to fall **(F)** Proportion of top performers. F = female, m = male.

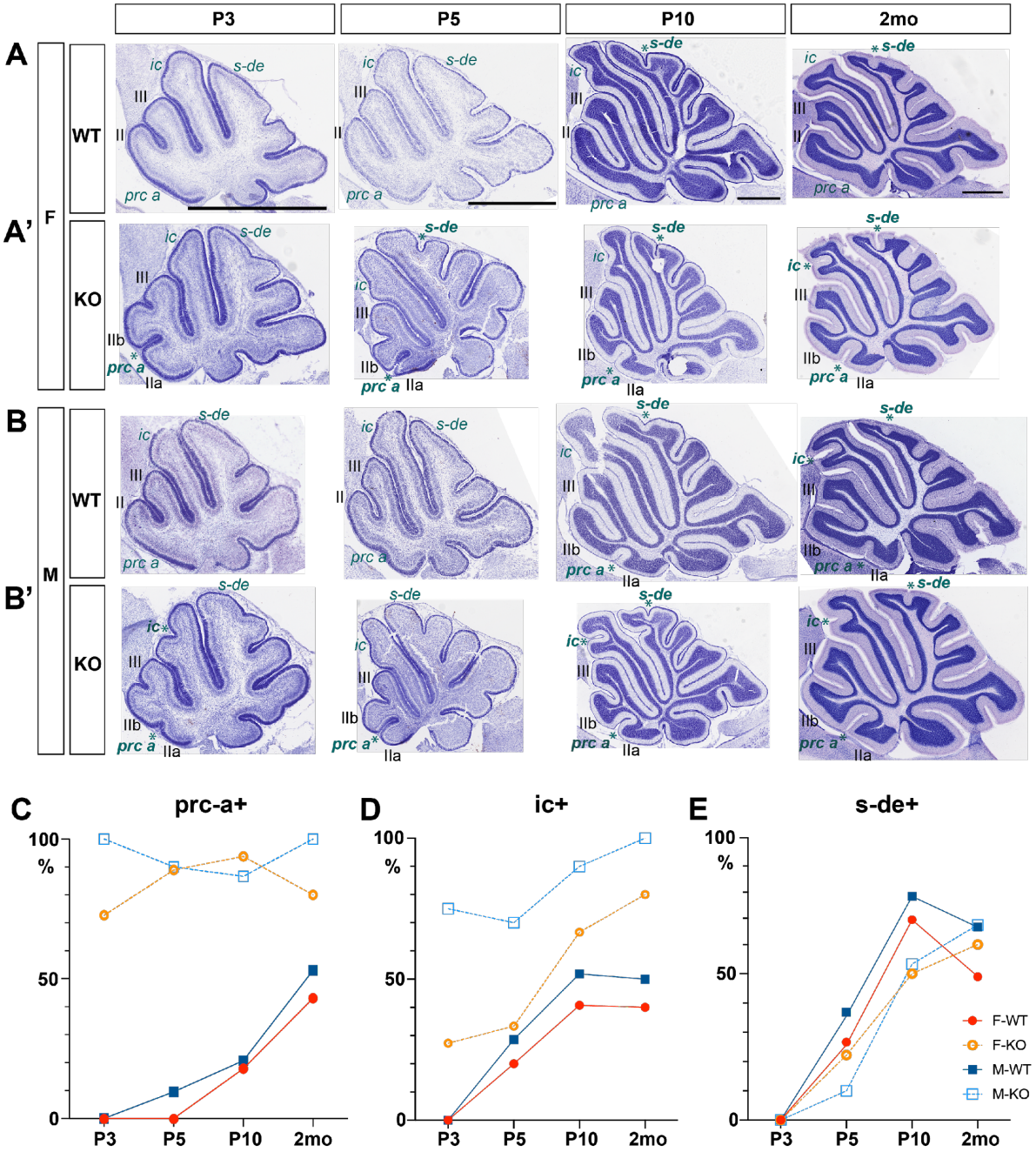

Figure 4. Cannabinoid Signaling Regulates Development of Secondary Fissures. Representative midvermal images from CD1 mice showing developmental timecourse of secondary fissure formation in **(A)** female wildtypes, **(B)** male wildtypes, **(A')** female knockouts, **(B')** male knockouts. **(C)** Quantification of the proportion of animals expressing ***prc-a*** at the different developmental timepoints. **(D)** Quantification of the proportion of animals expressing ***ic*** at the different developmental timepoints. **(E)** Quantification of the proportion of animals expressing ***s-de*** at the different developmental timepoints. Abbreviations: *ic* = intraculminate fissure, *pcen* = precentral, *prc-a* = anterior precentral fissure, *prm* = primary fissure, *s-de* = superior declive fissure, F = female, M = male, P = postnatal day.

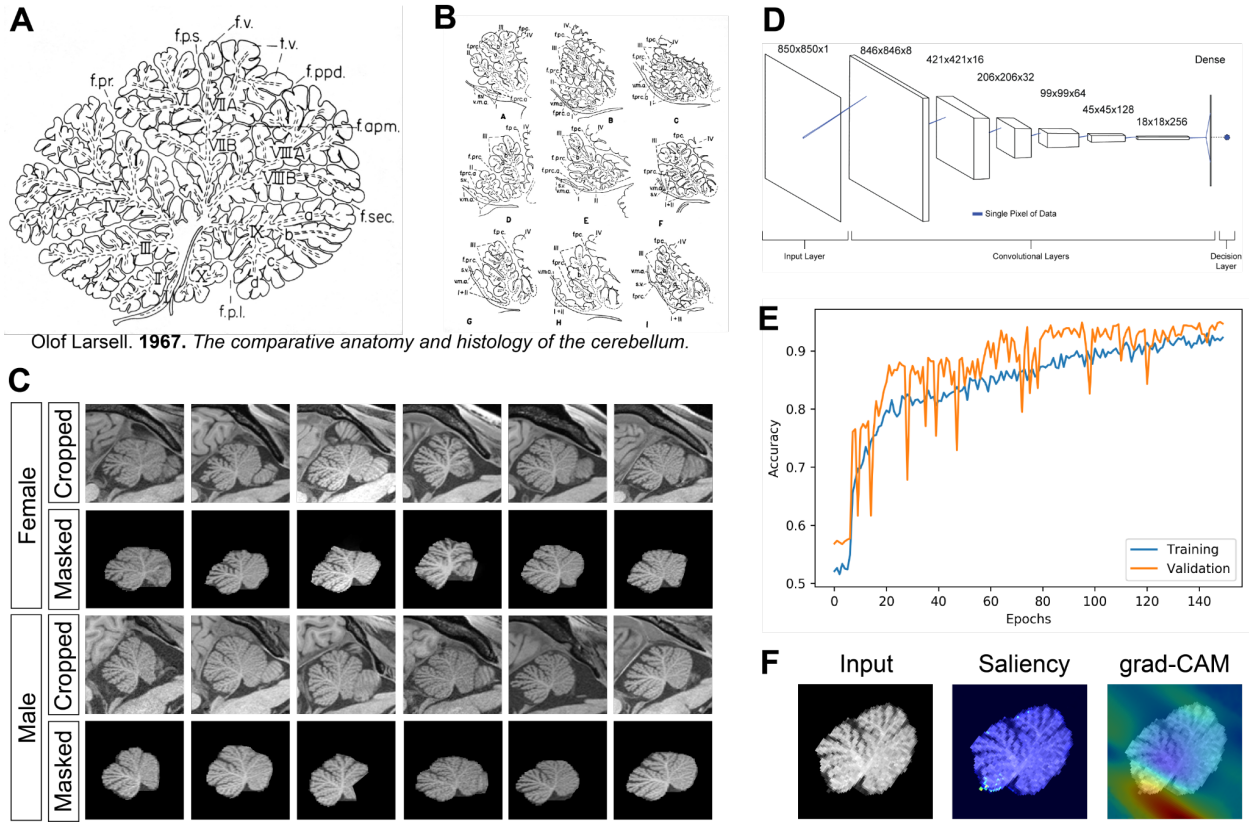

Figure 5. Human sex is well predicted using cerebellar anatomical images. (A) Traced midsagittal human cerebellar vermis with lobules and fissures marked (lobules I-X, rostral=left) from Olof Larsell's ***The Comparative Anatomy and Histology of the Cerebellum, Human Cerebellum,*** figure 55 B, p.45 (Larsell, 1967). **(B)** Figure 54, p.41 from (Larsell, 1967) illustrating the high degree of variability in anterior vermis folding. **(C)** Representative examples from HCP database of midline sagittal images. Images are shown in the same orientation as in (A). Top rows: images were selected through registering labels from the SUIT atlas to the subjects space, passed through an intensity normalization process that scaled the images for training (J. Diedrichsen et al., 2009, Jörn Diedrichsen, 2006, J. Diedrichsen et al., 2011), and hand cropped centering on the cerebellum to 850 pixels square. Bottom rows: images were masked and all pixels outside the label set were zeroed in order to limit analysis to midvermal cerebellum. **(C)** Deep convolutional neural network (CNN) was trained to predict biological sex cerebellar midvermis anatomy. The model was run for 500 epochs with 32 training and test steps per epoch. The filters initially describe the local patterns found in the image, but as the layers later in the model become smaller, they represent more global properties of the image. The decision layer used the combined weights from all the previous layers to make the desired category assignment. Prediction accuracy was used as a metric to evaluate model performance. **(D)** CNN was trained on 66% of the images (792 subjects), which were passed through a series of 6 2D convolutional filters and combined with pooling layers. Sex prediction was verified on the remaining 34% of the images (408 subjects). The accuracy for the training data never consistently surpassed the validation data, indicating the data is not over-fit and should generalize well to new samples. The best accuracy achieved was 93%. **(E)** Saliency of each voxel of the MRI in predicting sex (backpropagated heatmap) marking anatomical locations contributing the most to the sex-dependent differences, which highlighted the same anterior vermis variable lobules that the morphological analysis in mice identified as contributing to sex-dependent differences in folding.

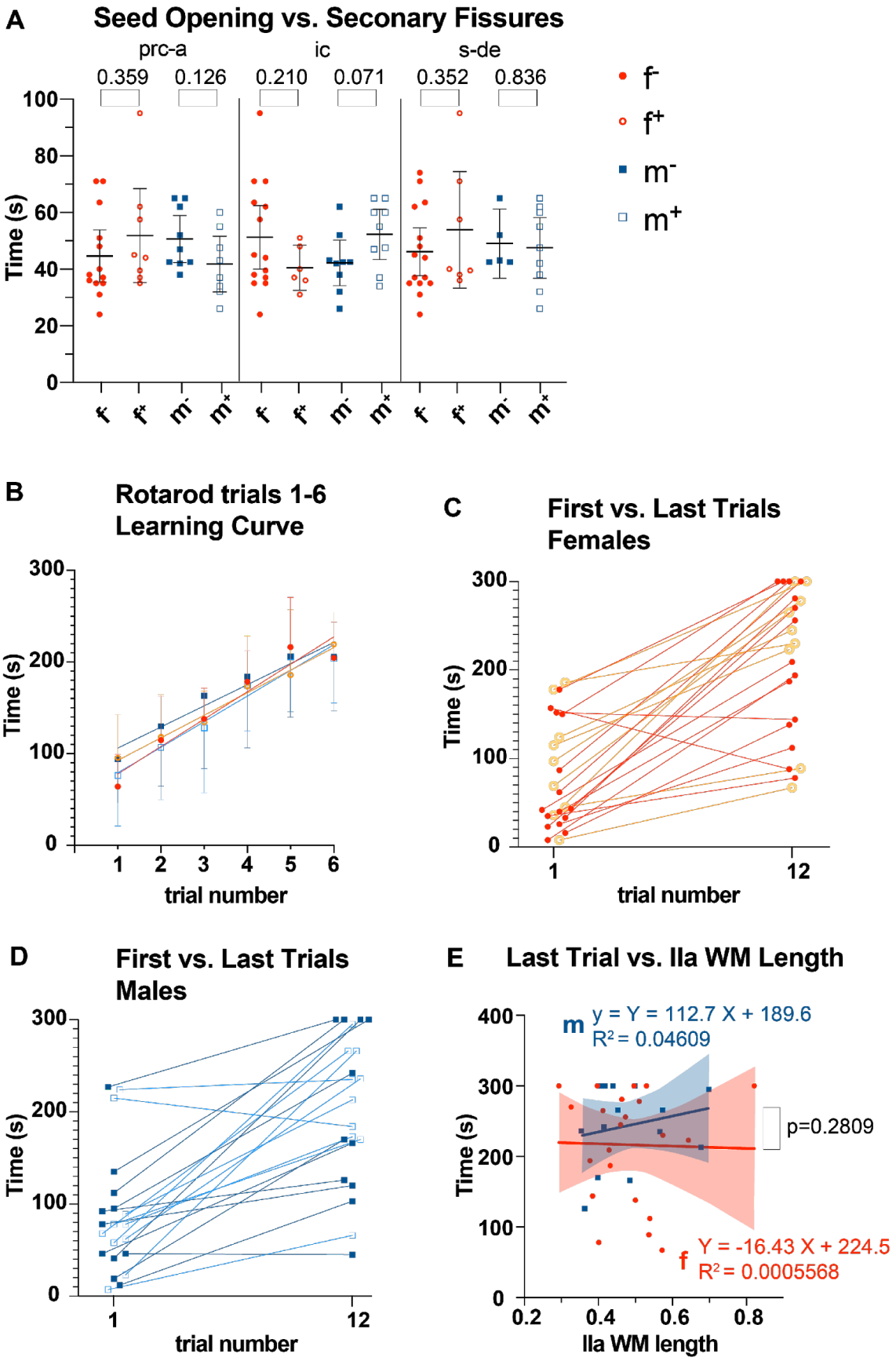
A
Seed Opening vs. Seconary Fissures
prc-a
ic
s-de
0.359
0.126
0.210
0.071
0.352
0.836
Time (s)
f-
f+
m-
m+
B
Rotarod trials 1-6
Learning Curve
Time (s)
trial number
C
First vs. Last Trials
Females
Time (s)
trial number
D
First vs. Last Trials
Males
Time (s)
trial number
E
Last Trial vs. IIa WM Length
m
y = Y = 112.7 X + 189.6
R² = 0.04609
p=0.2809
f
Y = -16.43 X + 224.5
R² = 0.0005568
Time (s)
IIa WM length

Supplemental Figure S-1. Shape versus function: behavioral measurements that do not exhibit clear correlation with sex and expression of secondary fissures. (A) Sunflower seed opening task. Y axis shows average time (in seconds) it takes a mouse to open a sunflower seed. Data is grouped by sex and expression of secondary fissures *prc-a, ic, s-de*. Mean differences in behavioral performance are not statistically significant between groups, and the range of variability in performance between individuals in any group is much larger than the differences between means, underscoring the likely presence of a multitude of additional factors influencing behavior. **(B)** Rate of learning for the first 6 trials in rotarod task. Latency to fall from the rod is shown on the Y axis. No differences are seen between sexes or between prc+ and prc- animals.**(C)** Improvement in rotarod from the first to the last trial for females, and **(D)** for males. No difference is seen between prc+ and prc- animals. **(E)** Regression analysis shows no clear correlation between IIa WM length and rotarod performance on the last trial.

References

Abel, J. M., Witt, D. M., & Rissman, E. F. (2011). Sex differences in the cerebellum and frontal cortex: roles of estrogen receptor alpha and sex chromosome genes. *Neuroendocrinology*, *93*(4), 230–240.

Bara, A., Ferland, J.-M. N., Rompala, G., Szutorisz, H., & Hurd, Y. L. (2021). Cannabis and synaptic reprogramming of the developing brain. *Nature Reviews. Neuroscience*, *22*(7), 423–438.

Chambers, W. W., & Sprague, J. M. (1955). Functional localization in the cerebellum. II. Somatotopic organization in cortex and nuclei. *A.M.A. Archives of Neurology and Psychiatry*, *74*(6), 653–680.

Coffman, K. A., Dum, R. P., & Strick, P. L. (2011). Cerebellar vermis is a target of projections from the motor areas in the cerebral cortex. *Proceedings of the National Academy of Sciences of the United States of America*, *108*(38), 16068–16073.

Corrales, J. D., Blaess, S., Mahoney, E. M., & Joyner, A. L. (2006). The level of sonic hedgehog signaling regulates the complexity of cerebellar foliation. *Development* , *133*(9), 1811–1821.

Diedrichsen, J. (2006). A spatially unbiased atlas template of the human cerebellum. *NeuroImage*, *33*(1), 127–138.

Diedrichsen, J., Balsters, J. H., Flavell, J., Cussans, E., & Ramnani, N. (2009). A probabilistic MR atlas of the human cerebellum. In *NeuroImage* (Vol. 47, p. S122). https://doi.org/10.1016/s1053-8119(09)71166-8

Diedrichsen, J., Maderwald, S., Küper, M., Thürling, M., Rabe, K., Gizewski, E. R., Ladd, M. E., & Timmann, D. (2011). Imaging the deep cerebellar nuclei: a probabilistic atlas and normalization procedure. *NeuroImage*, *54*(3), 1786–1794.

D'Mello, A. M., Crocetti, D., Mostofsky, S. H., & Stoodley, C. J. (2015). Cerebellar gray matter and lobular volumes correlate with core autism symptoms. *NeuroImage. Clinical*, *7*, 631–639.

Duan, D., Xia, S., Rekik, I., Wu, Z., Wang, L., Lin, W., Gilmore, J. H., Shen, D., & Li, G. (2020). Individual identification and individual variability analysis based on cortical folding features in developing infant singletons and twins. *Human Brain Mapping*, *41*(8), 1985–2003.

Hall, Z. J., Street, S. E., & Healy, S. D. (2013). The evolution of cerebellum structure correlates with nest complexity. *Biology Letters*, *9*(6), 20130687.

Inouye, M., & Oda, S. I. (1980). Strain-specific variations in the folial pattern of the mouse cerebellum. *The Journal of Comparative Neurology*, *190*(2), 357–362.

Jacobi, H., Faber, J., Timmann, D., & Klockgether, T. (2021). Update cerebellum and cognition. *Journal of Neurology*. https://doi.org/10.1007/s00415-021-10486-w

Kandel, E. (2013). *Principles of Neural Science, Fifth Edition*. McGraw Hill Professional.

Kim, B. J., & Scott, D. A. (2014). Mouse model reveals the role of RERE in cerebellar foliation and the migration and maturation of Purkinje cells. *PloS One*, *9*(1), e87518.

King, M., Hernandez-Castillo, C. R., Poldrack, R. A., Ivry, R. B., & Diedrichsen, J. (2019). Functional boundaries in the human cerebellum revealed by a multi-domain task battery. *Nature Neuroscience*, *22*(8), 1371–1378.

Larsell, O. (1967). *The Comparative Anatomy and Histology of the Cerebellum, from Myxinoids Through Birds: The human cerebellum, cerebellar connections, and cerebellar cortex*.

Legué, E., Gottshall, J. L., Jaumouillé, E., Roselló-Díez, A., Shi, W., Barraza, L. H., Washington, S., Grant, R. L., & Joyner, A. L. (2016). Differential timing of granule cell production during cerebellum development underlies generation of the foliation pattern. *Neural Development*, *11*(1), 17.

Legué, E., Riedel, E., & Joyner, A. L. (2015). Clonal analysis reveals granule cell behaviors and compartmentalization that determine the folded morphology of the cerebellum. *Development* , *142*(9), 1661–1671.

Martinez, L. R., Black, K. C., Webb, B. T., Bell, A., Baygani, S. K., Mier, T. J., Dominguez, L., Mackie, K., & Kalinovsky, A. (2020). Components of Endocannabinoid Signaling System

Are Expressed in the Perinatal Mouse Cerebellum and Required for Its Normal Development. *eNeuro*, *7*(2). https://doi.org/10.1523/ENEURO.0471-19.2020

Ma, S., Kwon, H. J., & Huang, Z. (2012). Ric-8a, a guanine nucleotide exchange factor for heterotrimeric G proteins, regulates bergmann glia-basement membrane adhesion during cerebellar foliation. *The Journal of Neuroscience: The Official Journal of the Society for Neuroscience*, *32*(43), 14979–14993.

McCarthy, M. M. (2016). Multifaceted origins of sex differences in the brain. *Philosophical Transactions of the Royal Society of London. Series B, Biological Sciences*, *371*(1688), 20150106.

Phillips, J. R., Hewedi, D. H., Eissa, A. M., & Moustafa, A. A. (2015). The Cerebellum and Psychiatric Disorders. In *Frontiers in Public Health* (Vol. 3). https://doi.org/10.3389/fpubh.2015.00066

Raz, N., Gunning-Dixon, F., Head, D., Williamson, A., & Acker, J. D. (2001). Age and sex differences in the cerebellum and the ventral pons: a prospective MR study of healthy adults. *AJNR. American Journal of Neuroradiology*, *22*(6), 1161–1167.

Sereno, M. I., Diedrichsen, J., Tachrount, M., Testa-Silva, G., d'Arceuil, H., & De Zeeuw, C. (2020). The human cerebellum has almost 80% of the surface area of the neocortex. *Proceedings of the National Academy of Sciences of the United States of America*, *117*(32), 19538–19543.

Sudarov, A., & Joyner, A. L. (2007). Cerebellum morphogenesis: the foliation pattern is orchestrated by multi-cellular anchoring centers. *Neural Development*, *2*, 26.

Whittaker, D. E., Kasah, S., Donovan, A. P. A., Ellegood, J., Riegman, K. L. H., Volk, H. A., McGonnell, I., Lerch, J. P., & Albert Basson, M. (2017). Distinct cerebellar foliation anomalies in aCHD7haploinsufficient mouse model of CHARGE syndrome. In *American Journal of Medical Genetics Part C: Seminars in Medical Genetics* (Vol. 175, Issue 4). https://doi.org/10.1002/ajmg.c.31595